Materials & Design 239 (2024) 112801

Contents lists available at ScienceDirect

Materials & Design

journal homepage: www.elsevier.com/locate/matdes

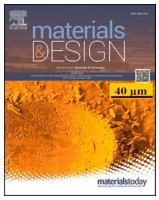

Combination of *ab initio* descriptors and machine learning approach for the prediction of the plasticity mechanisms in β-metastable Ti alloys

M. Coffigniez [a], P.-P. De Breuck [b], L. Choisez [a], M. Marteleur [a], M.J. van Setten [b,c], G. Petretto [b], G.-M. Rignanese [b], P.J. Jacques [a,*]

[a] UCLouvain, Institute of Mechanics, Materials and Civil Engineering, B-1348 Louvain-la-Neuve, Belgium
[b] UCLouvain, Institute of Condensed Matter and Nanosciences, B-1348 Louvain-la-Neuve, Belgium
[c] Now at IMEC, B-3001 Leuven, Belgium

ARTICLE INFO

Keywords:
β-metastable titanium alloys
Plasticity mechanisms
Machine learning
Ab initio
TRIP
Twip

ABSTRACT

This study proposes a machine-learning (ML) model combining *ab initio* calculations and an experimental dataset of 201 alloys (in addition to pure Ti) to predict the activated plasticity mechanisms in β-Ti alloys. This methodology is shown to be more efficient than the so-called $\overline{Bo}-\overline{Md}$ approach, achieving 82% prediction accuracy while the Bo-Md approach leads to 52% correct predictions on the same dataset. In addition, four new alloy compositions were produced to verify the model validity. Specific cases where the present model disagreed with the Bo-Md predictions were chosen to increase the benefits of the produced results. The plasticity mechanisms of the four alloys experimentally confirmed the validity of the ML model. This approach particularly helps the design of specific Ti alloys exhibiting a high work hardening rate owing to the simultaneous activations of the Transformation-Induced Plasticity (TRIP) and mechanical twinning (TWIP) effects. Indeed, the class corresponding to the combination of TRIP and TWIP effects reach a prediction accuracy of 88%.

1. Introduction

The design of new metallic materials remains an arduous task that relies on several sources of information or inspiration such as an experimental trial-and-error approach, phenomenological relationships or the results of calculations and simulations. It can be both time-consuming and expensive, particularly for breakthrough applications requiring new types of properties.

When designing new alloys, the first step is to consider the stability of the phase (or phases) resulting from the mixing of two or more elements. In order to guide this definition of stability conditions, numerous parameters have been proposed. The most used ones are the average number of valence electrons per atom (e/a), the ratio of atomic radii, the difference of electronegativity and the number of electronic vacancies [1], also still considered in the case of the very recent new paradigm of high entropy alloys [2]. Some of these guidelines are known as the *Hume-Rothery rules* [3] and are still very popular. These rules, which were initially based on empirical observations, state necessary conditions for (binary) solubilities and formation of intermetallic compounds. However, these rules give no clue about the properties, particularly the mechanical properties of the resulting solid solutions.

The next step in alloy design is to relate some characteristics of the alloys (global composition, crystal structure, evolution of solubilities, …) to activated mechanisms controlling the properties of interest such as strength, ductility, … in the case of structural properties. More or less empirical models are also generally used to guide the full procedure of property optimization.

For a few decades now, the "*d*-electron design strategy" introduced by Morinaga *et al.* [4] has been very popular, particularly in the case of designing new titanium alloys. Initially dedicated to the prediction of phase stability of multi-elements systems, this design approach was extended to predict the general trends in the modification of the Ti-β phase elastic properties [5–7], and more recently to design β Ti alloys exhibiting a large improvement of the work hardening capacity compared to classical Ti alloys [8–10]. This is achieved by combining, on the one hand, the calculation of two "electronic" parameters, i.e., the average bond order $\overline{Bo}$ and the average $\overline{d}$ level; and on the other hand, an empirical classification of plasticity mechanisms occurring in existing titanium alloys. As shown on Fig. 1, this two-parameter design tool is very convenient, represented as a map of phase stability and activated

* Corresponding author.
E-mail address: pascal.jacques@uclouvain.be (P.J. Jacques).

https://doi.org/10.1016/j.matdes.2024.112801
Received 24 July 2023; Received in revised form 22 February 2024; Accepted 24 February 2024
Available online 25 February 2024
0264-1275/© 2024 The Author(s). Published by Elsevier Ltd. This is an open access article under the CC BY-NC license (http://creativecommons.org/licenses/by-nc/4.0/).

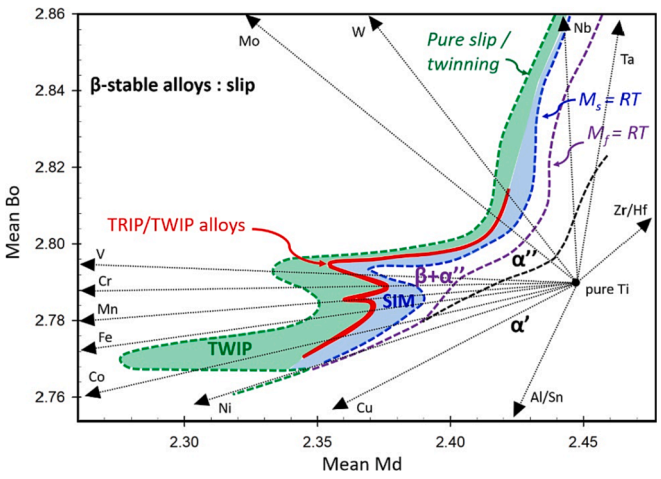

Fig. 1. Extended Bo-Md diagram for the design of TRIP/TWIP Ti alloys as presented in [8]. Each zone of the diagram corresponds to a particular plasticity mechanism.

Table 1
Limits of the Bo-Md approach: example cases of wrongly predicted plasticity mechanisms by the Bo-Md strategy.

Alloy composition (wt %)	Bo value	Md value	As quenched state and plasticity mechanism	
			Bo-Md prediction	*Experimental*
Ti-15Mo [11] *(Ti-7.79Mo at %)*	2.81127	2.40913	β-stable (dislocation glide)	β-TWIP
Ti-5553 [12,13] *(Ti-8.81Al-4.66 V-2.74Cr-2.38Mo at %)*	2.76483	2.36030	Martensitic (α')	TRIP
Ti-7.7Mo-4.7Co [14] *(Ti-4.01Co-3.88Mo at %)*	2.79011	2.36233	β-TWIP	Dislocation glide only (β)
Ti-10Mo-4Nb-2 V-3Al [15] *(Ti-5.6Al-5.04Mo-2.17Nb-1.98 V at %)*	2.79037	2.39682	Martensitic (α'')	β-TWIP + TRIP
Ti-35Nb-9.96Ta-4.53Zr [16] *(Ti-24.52Nb-3.58Ta-3.23 Zr at %)*	2.88800	2.46011	TRIP	Dislocation glide only (β)

plasticity mechanisms on which "alloy vectors" are drawn. Despite offering satisfactory results in many cases, this method also leads to wrong predictions as shown in Table 1.

The martensitic start temperature M_s has also often been used as a criterion to predict thermally induced or strain-induced martensitic transformation in Ti alloys [17,18]. The evolution of M_s was first empirically derived as a linear evolution of the alloying elements concentrations [19], then improved by a physically-based model by Bignon *et al.* [18], who associated thermal and strain-induced martensite transformations to different ranges of M_s values. However, they underlined that the activated deformation mode could not be solely predicted based on the M_s value and added an empirical criterion $[Fe]_{eq}$, defined as a linear variation of the concentration of the alloying elements, to predict the activated deformation modes. While their model constitutes a significant improvement of the "*d*-electron design strategy" for the prediction of strain-induced martensitic transformation, it is still semi-empirical and does not predict twinning-induced plasticity (TWIP).

Regarding the prediction of the TWIP effect, no physically based model has been derived to the best authors' knowledge; and the Bo-Md map is still mostly used to design TWIP Ti alloys [20]. Recently, Zhao *et al.* [21] derived a new energetic parameter to predict the plastic deformation mode of Ti alloys, based on a physical model very similar to the one derived by Bignon *et al.* [18]. This new parameter is defined as the difference between the driving force (chemical and mechanical) and the resistive force (elastic strain energy and frictional energy) to the martensitic transformation. However, their tool is not fully predictive as the mechanical properties have to be measured experimentally, or coupled with a model of the predicted mechanical properties of the alloy. Moreover, the model for the activation of the TWIP effect is also based on the physics of martensitic transformation. While a tendency between the predicted deformation mode and their energy parameter is highlighted, their prediction accuracy is only about 67 % [21]. As a summary, while physically based models contribute to a better understanding of the physics behind the deformation mechanisms of Ti alloys, no existing model fully grasps and estimates all the involved parameters in both TRIP and TWIP effects, and the predictive capacity of these models is still too low.

Another strategy is to improve the empirical criterion derived in the "*d*-electron design strategy". Recently, Wang *et al.* [14] proposed the use of two other parameters in addition to $\overline{Bo}$ and $\overline{Md}$ to predict the activation of twinning, martensitic transformation or dislocation glide during mechanical loading. These parameters are the average valence electron-to-atom ratio ($\overline{e/a}$) and the atomic radius difference ($\overline{\Delta r}$). The authors claimed that this alternative approach is able to predict accurately the behaviour of alloys incorrectly predicted by the $\overline{Bo}-\overline{Md}$ method. However, their conclusions are drawn with a unique example.

From a computational materials science viewpoint, the increase of computation facilities as well as the maturation of theories modelling condensed matter facilitate the accurate calculation of a variety of important quantities in design approaches like electronic band structures, phase stability, defects energies, etc. [22]. However, it is still difficult, not to say impossible, to deal with large systems without the use of several approximations.

Recently, machine learning (ML) has attracted considerable attention in materials science due to its ability to efficiently predict alloys properties with the assistance of physical-chemistry rules [23–25]. Supervised Machine Learning aims at establishing a model that represents a relationship between a collection of input data (as characterized by a set of descriptors) and the corresponding target (i.e., output property). The target can either be discrete (e.g., crystal structure) or continuous (e.g., melting temperature), which correspond respectively to a classification or regression task. Intrinsically, the size and quality of the input database strongly influence the prediction capability of a model, which could be an issue in the specific case of materials science. Indeed, as stated above, the generation of experimental results (alloys, properties, …) is time and energy consuming so that the size of the databases in materials science is mostly limited compared to other applications of ML (image analysis, natural language processing, information classification, etc.). As a consequence, predictions based only on the input database may lead to inaccurate or aberrant results. For this reason, ML is generally combined with relevant parameters related to the predicted properties. For example, Wen *et al.* [26] combined a ML algorithm with experimental design for processing high entropy alloys (HEAs) with high values of micro-hardness. Shen *et al.* [27] used physical metallurgy-guided ML algorithms with descriptors such as the equilibrium volume fraction and the driving force for precipitation, resulting in the successful design of advanced ultrahigh-strength stainless steels using only a small database extracted from the literature. Reddy *et al.* [28] established an inference model from compositions and heat treatment conditions to mechanical properties of low alloy steels by combining a neural network (NN) and genetic algorithm (GA). Their model successfully learns the influence of compositions and heat treatment conditions on the performance of the steel. Ozerdem *et al.* [29] built a multi-

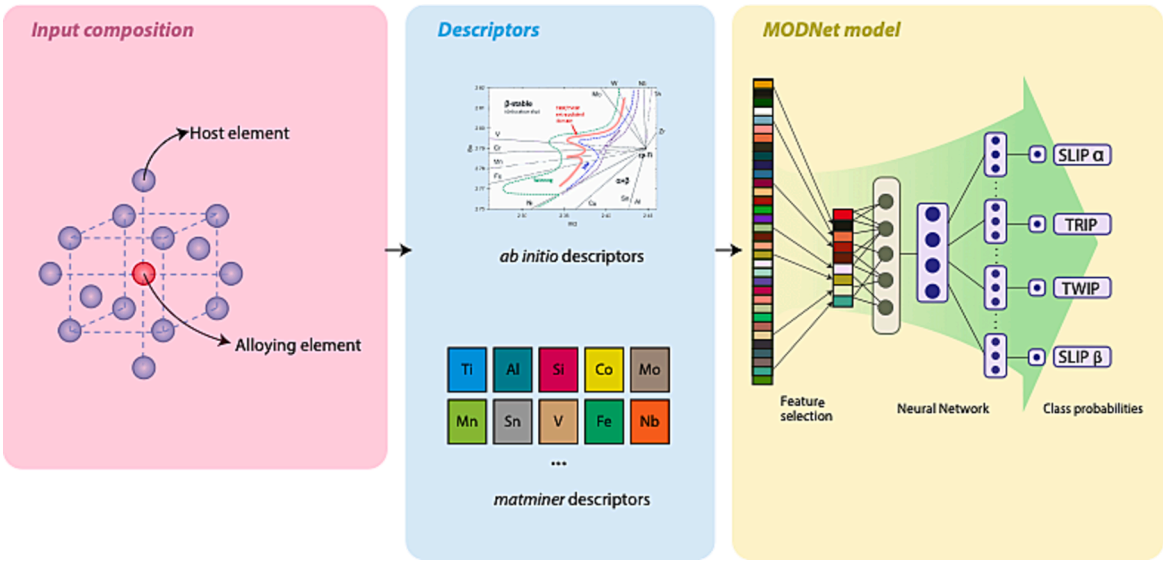

Fig. 2. Methodology for plasticity mechanism prediction. The design procedure consists of constructing a mixed database of calculated and experimental descriptors. MODNet model [30] is then applied to explore the compositional space of Ti alloys. The model returns the probability of activation for each plasticity mechanism as output.

layer BP NN model to predict the yield strength, ultimate tensile strength and elongation of the Cu–Sn–Pb–Zn–Ni alloy. Regarding titanium alloys, Wu *et al.* [30,31], created a NN to look for biocompatible chemical compositions that could lead to a Young's modulus below 50 GPa. To enhance the prediction of their model, they used the fact that lower moduli are usually reached when the β phase is retained. Therefore, they added a criterion on the Ms temperature and keep the output only for alloys presenting a Ms temperature below room temperature (meaning that β phase could be retained upon quenching). These NN models with inputs of compositions and processing conditions can provide an estimate of the properties of alloys. Such feedforward models from composition to property are helpful to screen for potential good candidates.

In this work, an original alloy design approach is proposed and applied to the prediction of the activation of plasticity mechanisms for specific compositions of Ti alloys, particularly to the design of TRIP-TWIP β-metastable Ti alloys. A large number of *ab-initio*- and composition-derived descriptors are associated with experimental results to develop a machine learning model thus combining continuous properties and discrete categories. It is worth noting that these mechanisms can be viewed as either a discrete or a continuous property depending on whether only the main activated mechanism is considered or the weight of each mechanism in the global plasticity response is considered. Here, we decided to regard each mechanism as a probability of occurrence.

2. Alloy design methodology

The general scheme of the proposed alloy design methodology is given in Fig. 2. It is based on a machine learning algorithm combining *ab initio* calculations of several parameters (that are detailed in Section 2.2), composition-based descriptors from matminer [32] and experimental results related to the phase stability and activated plasticity mechanisms. In the present particular case of designing Ti alloys

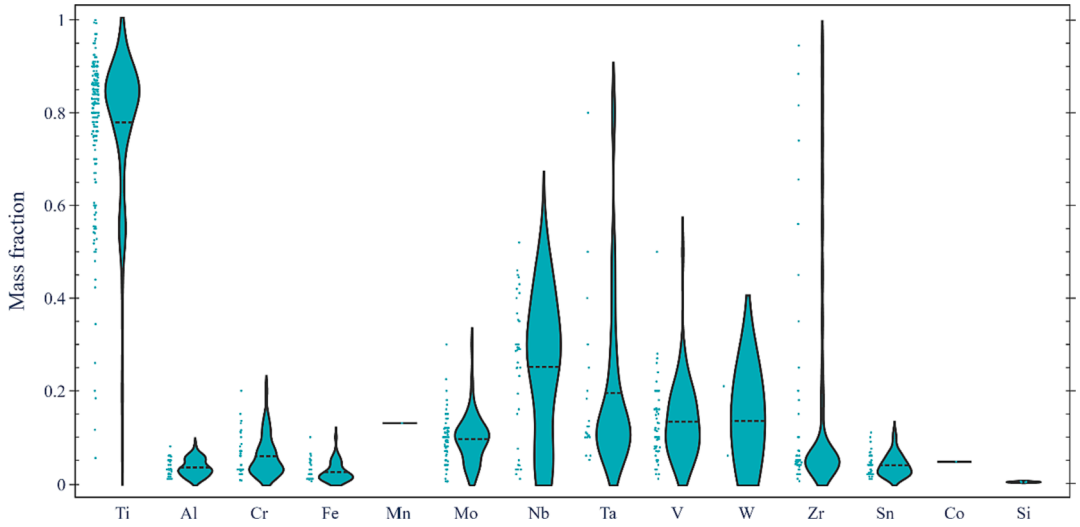

Fig. 3. Element distribution in the dataset. Violin plots representing the mass distribution over the different compounds, per element. Horizontal lines inside the distribution correspond to individual samples. All alloys are a mixture of Ti with other chemical elements present above. The range of mass fraction is a good indication on the expected generalization space of the machine learning model.

exhibiting improved work hardening properties, the aim is to predict specific alloy compositions presenting TRIP and / or TWIP effects, i.e., exhibiting β-metastable behavior, under quasi-static loading conditions. This study focuses on plasticity mechanisms only (irreversible), meaning that the TRIP effect is only considered as the formation of martensite upon loading without reversion to β upon unloading.

The dataset, descriptors and machine learning models are detailed below.

2.1. Dataset

The dataset contains 201 Ti alloys gathered from the literature, in addition to pure Ti as shown in Supplementary material (Table S3). There are 70 binary, 64 ternary, 39 quaternary, 20 quinary, 5 senary and 3 septenary compounds, respectively. Each sample is characterised by a chemical composition, plasticity mechanisms and an accompanying confidence weight, assigned according to the confidence that can be placed in the determination of the plasticity mechanisms (based on the conducted characterizations). The class "Slip α" refers to alloys exhibiting either hexagonal (h.c.p.) α' or orthorhombic α'' phases upon quenching from β domain. In these alloys, plasticity is only governed by dislocation glide. The classes "TWIP" and "TRIP" refer to β alloys at room temperature exhibiting respectively mechanical twinning or stress-induced martensitic transformation during loading. It is worth noting that the different twinning systems potentially activated in Ti alloys are not distinguished, because they are more rarely reported, and thus consequently would have reduced the size of the dataset. Finally, the "Slip β" class refers to β-stable alloys exhibiting dislocation slip only. They are the four labels of the classification task. It is also worth noting that some of them can occur simultaneously and that the concomitant activation of both TRIP and TWIP effects can bring improvements of the plasticity properties. Therefore, it will be modeled independently using a multi-label approach with four output probabilities. Depending on each probability level, the final prediction might be assessed as a combination of several mechanisms. This multi-label approach mimics the physics and results in a better model as will be shown.

Fig. 3 represents the fractional mass distribution of the different alloying elements present in the dataset. A palette of 13 elements is covered next to Ti: Al, Si, V, Cr, Mn, Fe, Co, Zr, Nb, Mo, Sn, Ta and W. Most elements span a narrow range below 30 wt %, with very few samples containing Si, Mn, Co, or W. Violin plots are used to visualise the training space. Prediction outside this chemical space (i.e. extrapolation) should be handled with caution, as they can lead to erroneous predictions.

2.2. Descriptors

The effectiveness of the machine-learning algorithm definitely relies on the appropriate choice of descriptors on which the training procedure is conducted.

A straightforward feature set can be formed by generating descriptors derived from elemental properties. Examples include statistics on the electronegativity, radii or mass of the constituent elements. To this end, matminer, a python package that gathers a wide variety of such descriptors was used [32]. It has been shown to be a good baseline for a variety of tasks [33]. Furthermore, as stated in the Introduction, we extended the feature space by also including *ab initio* descriptors.

Obtaining the actual *ab initio* descriptors for multi-component alloys would require the use of very large supercells. Moreover, for each new alloy or new prediction of an alloy, additional calculations would be needed. To circumvent this problem, in a way mimicking the approach proposed by Morinaga *et al.* with the $\overline{Bo}-\overline{Md}$ approach [4], the descriptors considered in the present study are approximated as linear combinations of the values calculated for binary Ti-X systems with a single concentration of several 'X'. More precisely, for a given host material and set of alloying elements, one cell of the pure host material and one cell where one host atom is replaced by one atom of the alloying element are constructed (see Fig. 2). The cells typically contain around sixteen atoms. For these cells of alloy element i, the descriptors $d_{i,j}$ were calculated, where j labels the descriptor. For a given alloy containing a specific mole fraction n_i of the alloying element i, the average descriptors are given by $d_j = n_i d_{i,j}$, assuming the summation convention. Note that while this linear approximation does not accurately represent the true value of that property, the obtained ab-initio-based descriptors constitute very interesting descriptors that help improving the machine-learning model, as we shall see.

All *ab initio* calculations were performed within density functional theory using a plane-wave basis-set. The exchange–correlation energy was modeled using the generalised gradient approximation functional proposed by Perdew, Burke and Ernzerhof [34]. Total energy calculations were carried using the VASP software within the projector augmented-wave methodology [35–37] with a plane-wave cutoff energy of 300 eV. The atomic positions and cell parameters were relaxed until all the forces were smaller than 0.01 eV/Å. Each alloying element X was considered as a substitutional defect in a 16-atom supercell of Ti. The corresponding formation energy is thus given by:

$$E_f(X) = E(X) - E(\text{bulk}) - \mu_X + \mu_{Ti}, \tag{1}$$

where $E(X)$ and $E(\text{bulk})$ represent the total energy of the supercell with and without the defect, while μ_X and μ_{Ti} are the element chemical potentials of the alloying element and of Ti, respectively. These values were extracted from the total energy of each element in its stable phase. For these calculations, the Brillouin zones are sampled with k-point grid with a density of at least 7000 points per reciprocal atom.

The same 16-atom supercell was used to calculate the position of the d-levels associated to the added alloying elements, M_d, as proposed by Morinaga to describe the elastic properties [6,38]. In the present case, this value corresponds to the first peak above the Fermi level of the projected density of states on the d states of the considered alloying element.

Additionally, stacking faults (SF) along the (1 1 0) plane were simulated with a supercell containing two shifted slabs and, due to periodic boundary conditions, two equivalent SFs. The (1 1 0) plane was chosen as it is one of the highest-packed planes in BCC crystals, hence often involved in twinning mechanisms [39]. Moreover, this plane limits the computation time compared to other highly packed planes such as (1 1 2). The generalised stacking fault energy (GSFE) can be defined as a function of the shift u

$$\gamma_{SF}(u) = (E_{\text{SF}}(u) - E(u=0))/2A, \tag{2}$$

where the energies $E_{\text{SF}}(u)$ and $E(u=0)$ represent the total energy of the supercell with and without the SF defect, A is the area of the surface and the factor 2 accounts for the presence of the two equivalent SFs in the supercell. By replacing one of the atoms at the location of the SF with one alloying element X and using a 2×2 supercell in the SF plane, the effect of X on the SF is considered as

$$\gamma_{SF}(u,X) = (E_{\text{SF}}(u,X) - E(u=0,X))/A - \gamma_{SF}(u). \tag{3}$$

It was verified that 8-layer slabs (16 layers in total) are enough to converge the energies. For this supercell, a $14 \times 14 \times 3$ k-point grid was used to sample the Brillouin zone. In this case, the atoms were allowed to relax only along the z axis. It was verified that different positions of X with respect to the SF do not provide additional independent descriptors.

The elastic tensor of the 16-atom supercell was also obtained for each alloy from density functional perturbation theory (DFPT) as implemented in the ABINIT software [40–43]. Optimised norm-conserving pseudopotentials [44] were used for all the elements treating semi-core states as valence electrons for transition metals (PseudoDojo

pseudopotentials table version 0.3 [45]). The cutoff was chosen independently for each material according to the values suggested in the Pseudo-dojo table. The Brillouin zone integration was performed using a $8 \times 8 \times 8$ k-point grid. All atoms were relaxed until all the forces on the atoms were below 5×10^{-6} Ha/Bohr and the stresses below 5×10^{-4} Ha/Bohr^3. The calculation of the relaxed-ion elastic tensor also requires the values of the phonon frequencies at Γ, that were obtained with DFPT calculations as well and whose values were also considered as possible descriptors.

All the calculations were automatised and analyzed using several python frameworks [46–50].

To summarise, the descriptors based on *ab initio* calculations are:

- *Bulk modulus K_V, K_R*: given the elastic tensor in the Voigt notation C_{ij} and the compliance tensor $s_{ij} = C_{ij}^{-1}$,

$$9K_V = C_{11} + C_{22} + C_{33} + 2(C_{12} + C_{23} + C_{31}) \tag{4}$$

$$1/K_R = s_{11} + s_{22} + s_{33} + 2(s_{12} + s_{23} + s_{31}). \tag{5}$$

- *Shear modulus G_V, G_R*:

$$15G_V = C_{11} + C_{22} + C_{33} - (C_{12} + C_{23} + C_{31}) + 3(C_{44} + C_{55} + C_{66}) \tag{6}$$

$$15/G_R = 4(s_{11} + s_{22} + s_{33}) - 4(s_{12} + s_{23} + s_{31}) + 3(s_{44} + s_{55} + s_{66}). \tag{7}$$

- *Poisson ratio* ν: $(3K_{VRH} - 2G_{VRH})/(6K_{VRH} + 2G_{VRH})$ where $K_{VRH} = (K_V + K_R)/2$ and $G_{VRH} = (G_V + G_R)/2$
- *Average phonon frequency* $\overline{\omega_\Gamma}$: Average of the phonon frequencies at the Γ point in meV.
- *Formation energy* E_f: defect formation energy of the alloying element in the 16-atom supercell in eV.
- *d-level* d_{max}: distance of the first *d*-level peak associated with the alloying element from the Fermi level in eV.
- *Averaged GSFE* $\overline{\gamma}_{SF}$: given 5 inequivalent shifts *u* in Eq. (3), we define

$$\overline{\gamma}_{SF}(X) = \sum_{i=1}^{5} \gamma_{SF}(u_i, X)/5. \tag{8}$$

Other theoretical features gathered from the literature have also been added. From Wang *et al.* [14] we included,

- *Average electron-to-atom ratio* $\overline{e/a}$
- *Average atomic radius difference* $\overline{\Delta r}$

and from the work of Morinaga *et al.* [4] we used the following electronic descriptors:

- Mean bond order $\overline{Bo}$
- Mean d-orbital energy level $\overline{Md}$

All the descriptors calculated by DFT (bulk modulus, shear modulus, Poisson ration, average phonon frequency, defect formation energy, d-level and average stacking fault energy) were obtained at 0 K and without considering the presence of oxygen. This may introduce a slight bias as Ti alloys of the dataset were tested at room temperature and may contain between 0.1 and 0.2 wt % of oxygen. However, as the estimation procedure of these descriptors remains the same for all the alloys, trends are preserved, and these descriptors can still be an aid to neural network predictions.

Table 2
ROC AUC scores for the different candidate models.

Model	Feature space	Slip β	Slip α	TWIP	TRIP	TWIP + TRIP
EHV	*ab initio*	0.88	0.98	0.77	0.67	0.79
ESV	*ab initio*	0.97	1.0	0.87	0.89	0.90
RF	*ab initio*	1.0	1.0	0.92	0.93	–
	matminer	1.0	1.0	0.91	0.92	–
	ab initio + matminer	1.0	1.0	0.92	0.94	–
MODNet	*ab initio*	1.0	1.0	0.95	0.96	–
	matminer	1.0	1.0	0.94	0.95	–
	ab initio + matminer	1.0	1.0	0.95	0.96	–

2.3. Machine learning model

The Material Optimal Descriptor Network (MODNet) [32] was used as the final classifier model. The model relies on a feedforward neural network and the selection of physically meaningful features. This reduces the optimization space without relying on a massive amount of data. MODNet has been shown to be very effective in predicting various properties of solids with small datasets [32,33].

An in-depth model selection procedure has been followed, where MODNet has been compared with different other strategies (as shown in the Results Section). The receiver operating characteristic curve enables to plot the true positive rate as a function of the false positive rate. A perfect model should detect all true positives before giving some false positives, leading to an area under the curve of 1. However, as it is not possible to reach perfect predictions, models usually start getting some false positives before having all the true positives, which decreases the area around the curve. This area under the receiver operating characteristic curve (ROC AUC) has been used as the evaluation metric (higher is better) on a repeated 5-fold.[1] MODNet yields the highest ROC AUC on this dataset, with the Random Forest being a close alternative (see Table 2).

Element-based statistics [32] combined with *ab initio* features systematically result in the highest ROC AUC. More information on the model selection can be found in the Supplementary material.

MODNet has been trained using a genetic hyperparameter optimization strategy, and ensembling is used [33]. Moreover, a multi-label approach has been adopted to better mimic the physics. In this scheme, the classes are independent (represented by a sigmoid output activation function), and a superposition of mechanisms is possible. The slip mechanism is therefore always present and the TWIP-TRIP mechanism can be combined, without introducing a fifth class. Finally, we also modified the loss function to include the confidence of each class, in order to obtain a weighted cross-entropy function:

$$L = \sum_{i \in C} F_i (p \log(\hat{p}_i) + (1 - p_i)\log(1 - \hat{p}_i)) \tag{9}$$

where C represents the set of classes, F the corresponding fidelity (trust weight given in Table S3), p the true class probability and $\hat{p}$ the predicted class probability. In essence, less importance is given to observations that were difficult to verify.

2.4. Processing and characterization of alloys

Some Ti grades were processed either for completing some unexplored zones of the $\overline{Bo} - \overline{Md}$ map, or for assessing the proposed alloy design procedure (see below). Raw materials of high purity (> 99.95%) were melted in an Arc 200 (Arcast Inc.) arc melting furnace under pure

[1] In a 5-fold validation scheme, each fifth of the database is used successively as a test set, with the remaining 4/5 used as a training base.

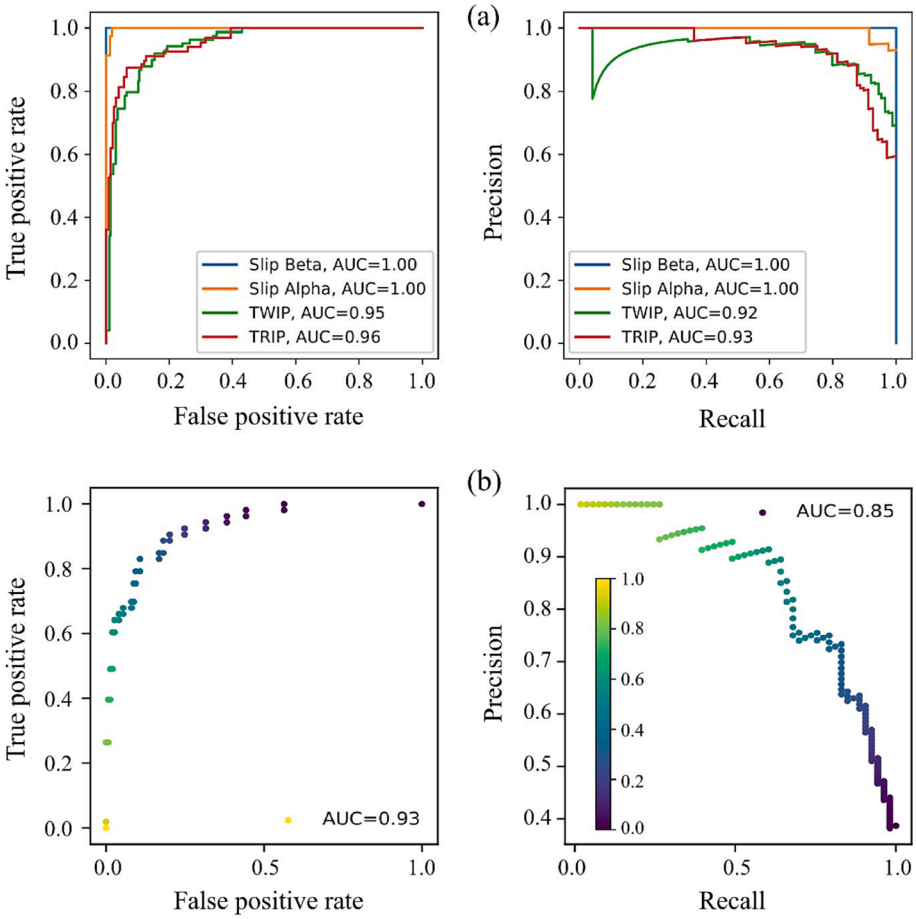

Fig. 4. Receiver Operating Characteristic (ROC) and Precision-Recall curves for the final model, i.e., MODNet with ab initio features, on the four classes (Slip β, Slip α, TWIP, and TRIP) (a), and on the combined TWIP – TRIP class (b). This class is formed by multiplying the separate TWIP and TRIP probabilities together. Corresponding thresholds are given by color. All the curves are computed over a 5-repeated 5-fold. The Area Under the Curve (AUC) is also given, with higher values corresponding to better performance.

Ar atmosphere. Each alloy was remelted several times to ensure chemical homogeneity and then cast in a copper mold. As-cast ingots (diameter of 12.7 mm) were annealed at 950 °C under Ar atmosphere for 30 min followed by water quenching. They were then cold-rolled down to 1 mm thick sheets. Uniaxial tensile specimens with a calibrated gauge length of 26 mm and a width of 6 mm were then obtained by Electrical Discharge Machining (EDM). Prior to tensile testing, the samples were recrystallised at 900 °C for 15 min under Ar atmosphere and water quenched to retain the full β microstructure.

Microstructures were characterised by X-ray diffraction before and after mechanical testing. Acquisitions were performed with a D8 Advance diffractometer (Brucker AXS GmbH), from 30 to 90° 2θ using Cu K α radiation, with current and voltage of 30 mA and 30 kV respectively, and a time step of 0.02°. Tensile tests were carried out at a displacement rate of 1 $mm.min^{-1}$ up to failure of the samples using a Zwick 50 kN tensile machine. In addition, one sample per alloy was also stopped after 5 % of strain to identify the occurrence of TRIP and / or TWIP effects by EBSD. To do so, strained samples were mounted in conductive resin and polished using SiC paper down to P4000, directly followed by 20 min of final polishing using a mixture of OP-S solution with 20 vol% hydrogen peroxide. The EBSD acquisitions were then performed in a FEG-SEM Ultra55 (Zeiss) using a Symmetry S3 EBSD detector (Oxford Instruments).

3. Results

3.1. Model selection

Different models were compared using a nested 5-fold validation scheme. Hyperparameters for each model are first individually optimised on an inner 5-fold. The best hyper parameters are then tested on the outer 5-fold. The following models were considered:

- Ensemble Hard Voting classifier (EHV): Ensemble of a Decision Tree, Random Forest, Support Vector Machine, K-Nearest Neighbours and a Multi-Layer Perceptron with a standard scaler. Hard voting, i.e., majority voting is applied. A multi-class approach is used, with twin-martensite being a separate class.
- Ensemble Soft Voting classifier (ESV): Ensemble of a Decision Tree, Random Forest, Support Vector Machine, K-Nearest Neighbours and a Multi-Layer Perceptron with a standard scaler. Soft voting, i.e., score averaging is applied. A multi-class approach is used, with twin-martensite being a separate class.
- Random Forest with multi-label approach.
- MODNet, with ensembling, multi-label and multi-fidelity approach.

Furthermore, while the feature space for the first two models only consists of *ab initio*- based parameters, as presented previously, the last two models also consider the features from matminer (composition based, magpie preset) and their combination with *ab initio*-based parameters. This makes a total of eight different algorithms that were

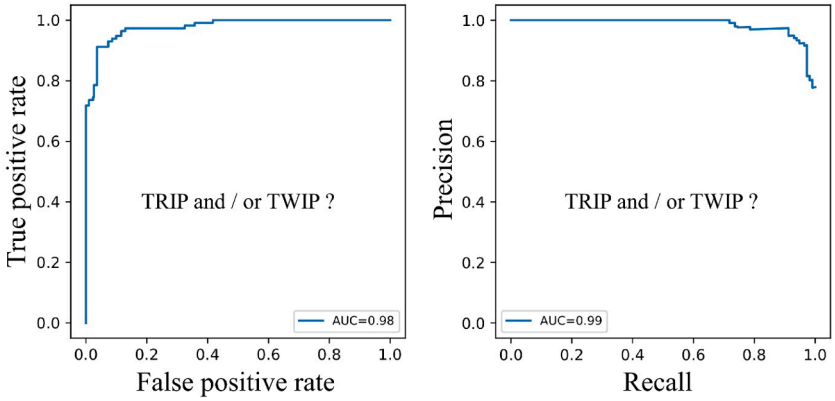

Fig. 5. Receiver Operating Characteristic (ROC) and Precision-Recall curves for the binary prediction (β-metastable or not). Curves are computed over a 5-repeated 5-fold. The Area Under the Curve (AUC) is also given, with higher values corresponding to better performance.

tested on the whole database.

Table 2 shows the ROC AUC scores of the nested cross validation for each class (Slip β, Slip α, TWIP, TRIP). The ROC curves can be found in Supplementary material, Fig. S1.

It is seen how ESV is superior to EHV. Moreover, the continuous output gives more interpretability (probability score). Next, all multi-label approaches outperform the multi-class approach, confirming that the multi-label approach better corresponds to the physics of the deformation modes selection in Ti alloys. Considering the Random Forest, it is seen that the *ab initio* and matminer features result in the highest scores, although different feature spaces being quite close to each other. Similarly, MODNet results in the highest score when using combined *ab initio* and matminer features (although the ROC AUC is similar, it has a slightly higher precision-recall AUC). It is the overall best performing model and is therefore used in the remainder of this work. This can be explained by the feature selection procedure, non-linearity of the neural network and customised loss function.

In summary, MODNet with the complete feature space (*ab initio* + matminer) is chosen as it results in the highest ROC AUC score. However, the RF with *ab initio* features is close in performance, while being computationally easier, and might thus be considered as an alternative.

3.2. Machine learning predictions

MODNet automatically identified the important descriptors by accounting for relevance and redundancy. This enables one to better interpret the model. Based on the normalised mutual information, it is found that the elastic properties (G_V, G_R, ν), the electron to atom ratio ($\overline{e/a}$) and the stacking fault energy ($\overline{\gamma_{SF}}$) are the most relevant *ab initio* descriptors with respect to the target. It makes sense as both the electron to atom ratio and the elastic properties are directly involved in the physics of phase transformations [18,21,51–54] and the stacking fault energy is the most important parameter involved in twinning induced plasticity [55]. Intriguingly, $\overline{Bo}$ and $\overline{Md}$ have the lowest importance of all features. While Bo and Md were originally used to predict the phase stability of Ti alloys, the extension of their use to the prediction of its deformation modes is only empirical. This lack of physical significance or underlying theory may explain the low importance of these parameters in the MODNet model. Among the composition-based matminer descriptors, it is found that the column number and d-valence electrons play an important role in the predictions. These provide indications on the kind of the bonds occurring in the compounds.

Moreover, (B_R, B_V) and (G_R, ν) were found to be highly related, while all other descriptors have a low similarity. In particular, G_V and $\overline{\Delta r}$ are found to be important complementary features to the model. It is therefore interesting to note how both the *ab initio* and matminer features play an important role for the predictions.

Fig. 4 (a) represents the ROC and precision-recall (PR) curves of the ML model for the Slip β, Slip α, TWIP, and TRIP classes, respectively. Precision is the ratio of correctly predicted positive instances to the total predicted positive instances. It measures the accuracy of positive predictions. Recall is the ratio of correctly predicted positive instances to the total actual positive instances. It measures the ability to capture all positive instances.

In practice, when aiming to minimize false positives (instances detected as TRIP-TWIP while they are not), one should prioritize achieving a high precision. Conversely, when aiming to avoid missing any potential TRIP-TWIP candidates, a higher recall becomes crucial. These two metrics typically trade off against each other.

Excellent performance is found on the Slip β and Slip α classes (with a 1.00 AUC). The ROC AUC for TWIP and TRIP are 0.95 and 0.96, respectively, which is lower than the previous classes, but significantly above random (0.5). The PR-curve confirms this but depicts a more realistic view by including the precision. Due to the one – versus - all approach, imbalance is present, and lower precision values can be expected. Note that one can expect even better performance with increasing dataset size.

However, plasticity of some alloys can simultaneously involve TRIP and TWIP effects. Fig. 4 (b) represents the ROC and PR curves corresponding to a heuristic multiplying the predicted twin and martensite scores, with an AUC of 0.93. This can be seen as the probability of the combined occurrence of both phenomena. Thresholds are depicted by coloring the corresponding false and true positive rates. The maximum accuracy (0.88) is found for a threshold of 0.34, which lead to a precision and recall of 0.72 and 0.83, respectively. This forms a good compromise between the different metrics. If one seeks precision, increasing the threshold to 0.7 increases the precision to 0.93 but reduces the recall to 0.49. On the other hand, decreasing the threshold to 0.1 will increase the recall to 0.94 while decreasing the precision to 0.50.

Finally, in practice, it might be useful to individually investigate and assess the different probabilities for a global understanding. The model gives the probability of occurrence for each mechanism. It has the advantage of being interpretable compared to a hard classifier. A thresholding heuristic is applied to extract the final mechanism: if combined occurrence (i.e. product of probabilities) of both TWIP and TRIP is higher than 34 %, we predict it as such. Otherwise the class that exceeds a probability of 50 % is predicted. The dislocation glide can be present in addition to another mechanism if one of them exceeds the threshold, or alone if all the other probabilities remain below 0.5. Following this scheme leads to a prediction accuracy of 82 %. As a comparison, the accuracy of the Bo-Md approach on the same dataset is 52 %.

In some cases, alloy designers may only be interested in the potential

Table 3
Some examples of misprediction using the repeated 5-fold validation scheme. Predictions are given as probability scores for each class: Slip β, Slip α, TWIP, and TRIP. Although the thresholding applied results in poor predictions, the calculated probabilities remain consistent with the experimental observations.

Composition (wt %)	Slip β	Slip α	TWIP	TRIP	Threshold heuristic	$\overline{Bo}-\overline{Md}$	Experiment
Ti – 11.5Cr [56]	1.00	0.02	**0.57**	0.03	TWIP	TWIP	**Slip β**
Ti – 9.3Mo – 4.6Sn [57]	1.00	0.00	0.39	**0.95**	TWIP + TRIP	Slip α	**TRIP**
Ti – 14Mo [58]	1.00	0.00	**0.97**	0.39	TWIP + TRIP	Slip β	**TWIP**

metastability of the alloy. Fig. 5 represents the ROC and PR curves of the ML model for the binary prediction: "is this alloy β-metastable (TRIP and / or TWIP) or not?". By reducing the number of classes to two (metastable or not), the accuracy of the model reaches 93 % (against 64 % for $\overline{Bo}-\overline{Md}$). In addition, the AUC scores for both the ROC and PR curves are increased to excellent performance of 0.98 and 0.99 respectively, as a result of the larger number of alloys per class.

In summary, the model clearly distinguishes the observed effects, and although it is not perfect, it clearly outperforms the $\overline{Bo}-\overline{Md}$ approach. It is remarkable to see that despite the limited amount of data, good performance is achieved and will continue to improve with the size of the dataset.

4. Validation and discussion

The assessment of the predictions of the ML algorithm fed with *ab initio*-calculated descriptors for Ti alloys and a rather limited set of experimental data points show that effective predictions can be reached. It is worth noting that the prediction success for binary alloys is particularly interesting, reaching an accuracy of 92.7 % with the ML prediction against 70.6 % for the $\overline{Bo}-\overline{Md}$ approach. Moreover, some mispredictions are directly linked to a lack of data in some regions of the chemical space, as with Ti-21 W, which is incorrectly predicted because only two alloys contain tungsten in the database.

Another important point to highlight is that 77 % of the wrong predictions are linked to the inaccuracy of the model in locating the exact position of the boundary between two mechanisms. In these specific cases, the probabilities of occurrence given for each mechanism by the model can warn us of a possible low confidence of the model at that boundary. For example, Table 3 shows 3 mispredicted alloys for which the calculated probabilities are just above the threshold to toggle from one mechanism to another but the probability distribution still illustrates the confidence level of the model on each mechanism. Indeed, the TWIP probability for Ti-11.5Cr is only slightly above the 0.5 threshold, meaning that the confidence in TWIP occurrence in this alloy is really low. Similarly, for both Ti-9.3Mo-4.6Sn and Ti-14Mo, the product of TRIP and TWIP probabilities slightly exceeds 0.34, leading to a classification of these alloys as TWIP + TRIP. However, this value is reached with a strongly unbalanced probability distribution between TRIP and TWIP mechanisms, in favor of TRIP for Ti-9.3Mo-4.6Sn and TWIP for Ti-14Mo, which corresponds to what is experimentally observed. It should also be noted that 2/3 of the mispredictions due to domain boundaries concerns the distinction between the occurrence of only one or both phenomena (TWIP + TRIP) within the β-metastable domain. We therefore strongly encourage the user to analyze and interpret the individual probabilities to form a global picture of the prediction instead of relying on hard boundaries.

It is also interesting to highlight that some specific alloying elements are particularly strongly represented among the misclassified alloys. This is notably the case for Sn and Zr. Concerning Zr, it should be pointed out that it is considered as a neutral alloying element in titanium, in the sense that it does not affect the beta transus temperature. However, its effect in the case of β-metastable alloys is still not fully understood and depends on the quantity of other β-stabilizing elements, as shown by Abdel-Hady *et al.* [59]. Indeed, Zr was shown to increase the martensite start (M_s) temperature in Ti-Ni system [60], decrease M_s in Ti-Nb system [59,61,62], while not impacting the deformation mode in both Ti-Cr and Ti-V systems [63]. Moreover, the addition of 3 wt % of Zr in Ti12Mo changes the deformation mode from TRIP + TWIP to TRIP only, while a further increase of the Zr content up to 10 wt % leads to TWIP only [64]. These results highlight the need of further investigation of the influence of Zr on the deformation modes in β-metastable Ti alloys, with a physical origin that is probably not included yet in the parameters used for this ML model. Concerning Sn, 71 % of the mispredicted alloys containing Sn without the presence of Zr are included in the database with a confidence weight of less than or equal to 0.5. These low confidence weights are due to the lack of complete characterization of these alloys in the literature, decreasing the confidence in the presence or absence of certain plasticity mechanisms. The mispredicted alloys by the model are thus a way to highlight either where deeper assessment or characterisation is still required or where errors might have been reported in the literature.

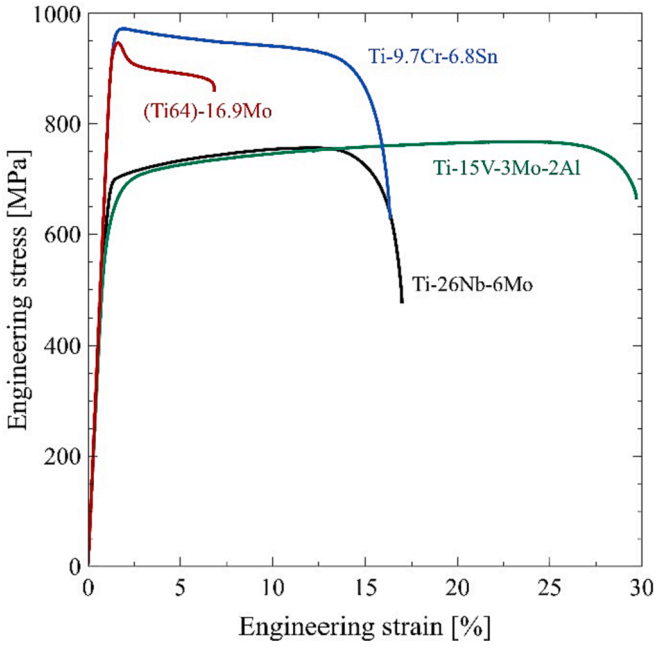

Fig. 6. Engineering stress - strain curves of the new investigated alloys.

Finally, it is worth emphasizing that the predictions are largely improved with respect to the $\overline{Bo}-\overline{Md}$ approach. However, to complete this assessment of the right prediction of the different modes of plasticity in Ti alloys, 4 new grades were processed and tested. These specific compositions were explicitly chosen to challenge the $\overline{Bo}-\overline{Md}$ approach (see Supplementary Material Fig. S2 for their locations on the $\overline{Bo}-\overline{Md}$ map):

(i) 83.1 (Ti-6Al-4 V) – 16.9 Mo alloy, called Ti64-Mo in the following, was designed by modifying the Ti-6Al-4 V alloy to reach the theoretical TRIP/TWIP locus;

(ii) Ti-9.7Cr-6.8Sn is an *iso*-elements modification of the Ti-8.5Cr-1.5Sn TRIP/TWIP alloy [10] still laying on the TRIP/TWIP locus;

(iii) Ti-26Nb-6Mo lies in a zone of the $\overline{Bo}-\overline{Md}$ map where fewer data points were reported;

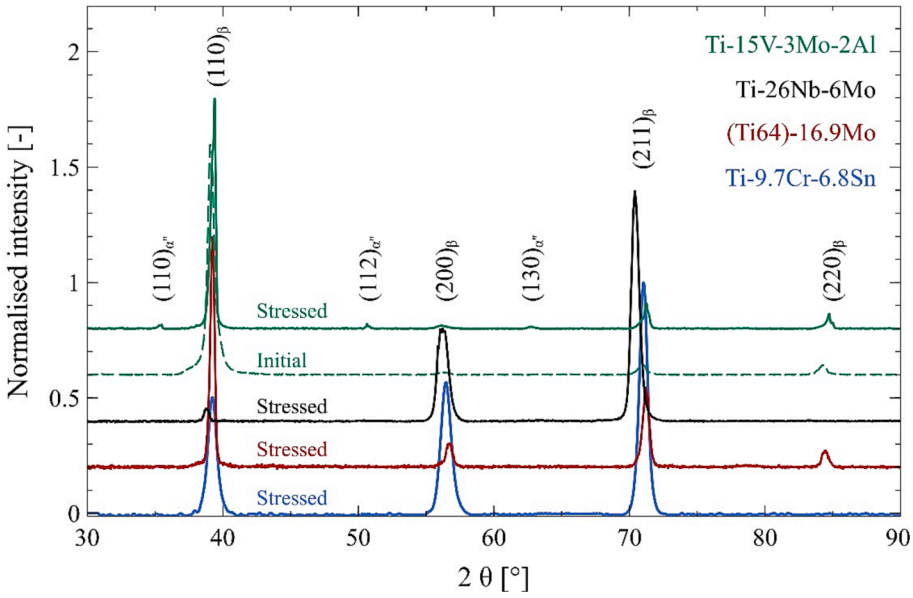

Fig. 7. X-ray diffraction patterns of the alloy compositions tested in this study after straining up to failure, in addition with the initial state pattern of the only sample that present martensite after fracture.

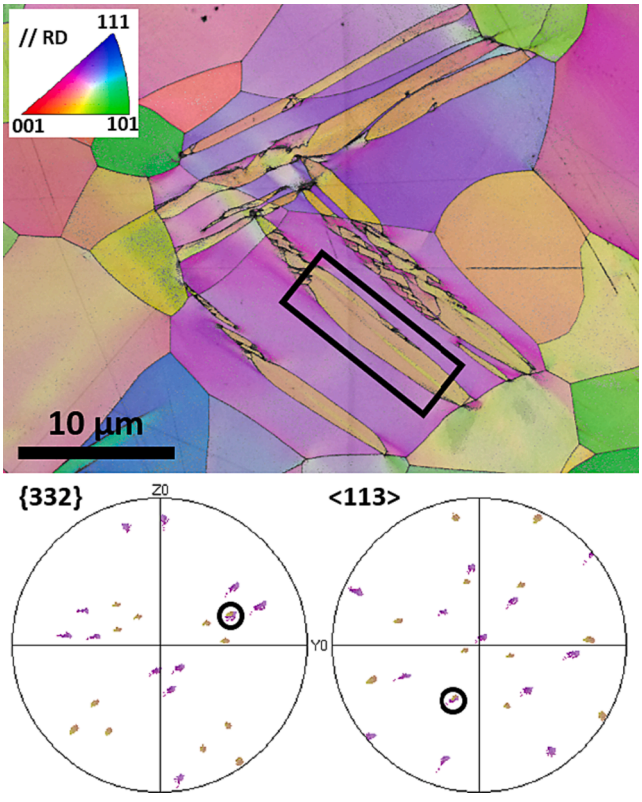

Fig. 8. Inverse pole figure of Ti-26Nb-6Mo alloy strained up to 5 % illustrating the presence of deformation bands. Associated pole figures highlight the {3 3 2} ⟨1 1 3⟩ twinning relationship of the deformation band present in the black rectangle.

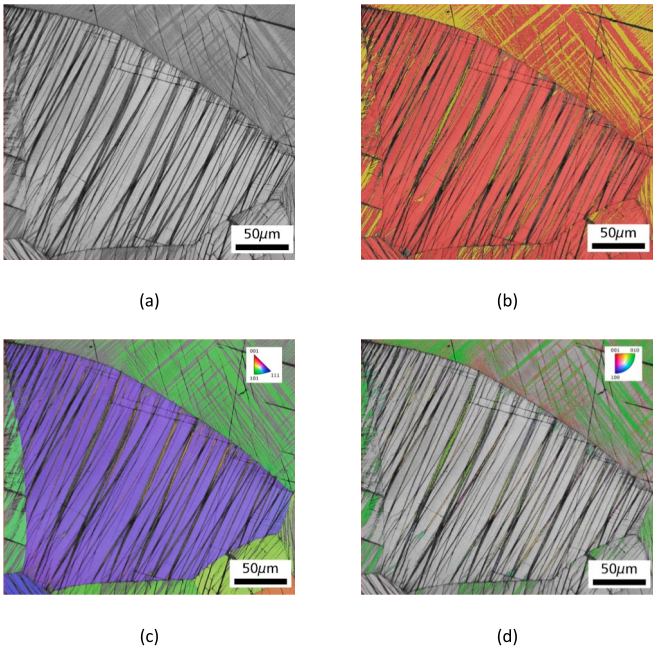

Fig. 9. Band contrast (a), phase map (with BCC phase in red and α'' in yellow) (b), and inverse pole figures of BCC (c) and α'' martensite (d) of Ti-15V-3Mo-2Al alloy strained to 5 %. (For interpretation of the references to color in this figure legend, the reader is referred to the web version of this article.)

(iv) Ti-15V-3Mo-2Al alloy was designed as a predicted TRIP/TWIP alloy located in the slip region of the $\overline{Bo}-\overline{Md}$ map;

The tensile curves of the 4 designed alloys are gathered in Fig. 6. Two different behaviours can be clearly identified. On the one hand, 2 alloys, Ti64-Mo and Ti-9.7Cr-6.8Sn, exhibit a very high yield strength together with no work-hardening capacity, which is classically the mechanical behaviour of β-stable Ti alloys with plasticity driven by dislocation glide, leading to a flow stress continuously decreasing after the yield point. On the other hand, the 2 other alloys (Ti-26Nb-6Mo and Ti-15V-3Mo-2Al) exhibit some work-hardening during tensile straining. This behaviour suggests the activation of TRIP and/or TWIP effects.

Fig. 7 presents the X-ray diffraction patterns after fracture of the different tested alloys in addition to the diffractogram of the Ti-15V-3Mo-2Al alloy in its initial state. All grades exhibit a fully β microstructure prior to straining. These diffractograms confirm that, except for the Ti-15V-3Mo-2Al alloy, no other phases were present after tensile testing. In the case of the Ti-15V-3Mo-2Al alloy, diffraction pattern

Table 4
Predictions of plasticity mechanisms for challenging designed alloys. Predictions are given as probability scores for each class: Slip β, Slip α, TWIP, and TRIP. A thresholding heuristic is applied to find a final mechanism: either the class with the score above 0.5 (in addition to slip) or TWIP - TRIP if their product exceeds 0.25. Comparison is made with the $\overline{Bo}-\overline{Md}$ approach and the experimental validation.

Composition (wt %)	Slip β	Slip α	TWIP	TRIP	Threshold heuristic	$\overline{Bo}-\overline{Md}$	Experiment
(Ti-6Al-4 V)83.1 – 16.9Mo	1.00	0.02	0.00	0.00	Slip β	TWIP + TRIP	Slip β
Ti-9.7Cr-6.8Sn	1.00	0.00	0.05	0.00	Slip β	TWIP + TRIP	Slip β
Ti-26Nb-6Mo	1.00	0.00	0.52	0.02	TWIP	Slip β	TWIP
Ti-15V-3Mo-2Al	1.00	0.00	1.00	0.90	TWIP + TRIP	Slip β	TWIP + TRIP

exhibits α'' reflections, suggesting the occurrence of the TRIP effect.

Scanning Electron Microscope (SEM) observations did not reveal any trace of strain-induced interfaces such as twin boundaries in Ti-9.7Cr-6.8Sn and Ti64-Mo samples, confirming the β-stable nature of these grades. Concerning Ti-26Nb-6Mo and Ti-15V-3Mo-2Al alloys, the nature of the observed strain-induced bands was investigated by EBSD. Fig. 8 shows that mechanical twinning occurs during the deformation of the Ti-26Nb-6Mo grade. Indeed, deformation bands corresponding to {332} ⟨113⟩ mechanical twins, the common twinning system in metastable β-Ti alloys [8,10], are present. It also confirms the XRD results where no additional α'' peaks were observed after straining.

On the other hand, the different maps of Fig. 9 show that both mechanical twinning and strain-induced martensite occur in the Ti-15V-3Mo-2Al alloy, also in agreement with the XRD results. Indeed, deformation bands are indexed either as mechanical twins or strain-induced martensite.

The probabilistic predictions of the proposed Machine Learning model are presented in Table 4, together with the ones of the $\overline{Bo}-\overline{Md}$ approach and the experimental results obtained via tensile testing and subsequent microstructural characterization. It can be seen that the predictions of the present model are globally much better than the phenomenological approaches of Morinaga and Wang, despite the relatively small number of input data. The new approach accurately predicts the activated plasticity mechanism for all the different cases, while the $\overline{Bo}-\overline{Md}$ approach is completely unable to correctly predict any of these challenging compositions. Moreover, one strength of the present approach compared to previous attempts is the potential of continuously improving the capacity of the predictor, which is intrinsic to the machine-learning concept. It is also worth noting that none of the other approaches summarized in the Introduction would be able to predict the activated plasticity mechanisms as globally and accurately as the present approach.

5. Conclusions

We presented in this work an original approach for the design of β titanium alloys exhibiting specific plasticity mechanisms. Based on an approach initiated by Morinaga *et al.* linking electronic parameters and observations of plasticity mechanisms, a hybrid machine learning model combining ab initio calculations and a set of experimental data was built and validated. Among the different algorithms tested in this study, a multilabel and multi-fidelity MODNet trained on *ab initio* and matminer features showed the best results. A probabilistic approach was chosen, as it showed better performance compared to a hard-voting algorithm (see Supplementary material). This enables task-specific thresholding (e.g., when high recall or precision is needed) and, furthermore, enables active learning strategies. The multilabel approach has the advantage to better represent the physics, by dealing with separate independent classes. As a result, better scores were obtained and the interpretation was easier. Moreover, it can be observed that the domain-specific *ab initio* features (although with strong simplifications, i.e., linearly extrapolated) provide a strong descriptive behaviour, and outperform standard features such as the ones available in matminer.

Moreover, this new tool can constantly be improved by the addition of new experimental points in the dataset, improving the accuracy of the predictions. An interface to access the predictions of the developed model is also available online [65]; any kind of experimental data of correct or wrong predictions can be provided to the authors to be included in the training database.

This new approach has been demonstrated to handle some limitations of the widely used $\overline{Bo}-\overline{Md}$ design map, especially in its main current use, i.e., the design of new Ti alloys with an improved work hardening rate through the activation of the TRIP and TWIP effects.

The present approach also started to guide deeper understanding of the fundamental mechanisms responsible for the activated plasticity mechanisms. Indeed, the statistical analysis of the strength of the correlations established between ab initio-calculated electronic parameters and observed plasticity mechanisms reveals which parameters have a predominant effect. It could also be extended to a larger panel of properties as long as valid experimental data points are available for the initial training of the machine learning algorithms. However, despite predicting accurately the activated plasticity mechanisms in β-Ti alloys, the model is currently unable to assess the intensity with which each phenomenon takes place. Since it can be anticipated that the work hardening capacity relies on the density of twins or laths created, if two alloys exhibit the same plasticity modes, the model cannot predict which one will have a higher strain-hardening capacity. Further improvements should deal with complementary criteria or better understanding of the underlying parameters dictating mechanical properties such as uniform elongation and/or ultimate tensile strength. In the case of TRIP/TWIP Ti alloys, next improvements will consist in adding output properties such as yield strength, uniform elongation or fracture toughness for example.

CRediT authorship contribution statement

M. Coffigniez: Conceptualization, Investigation, Validation, Visualization, Writing – original draft, Writing – review & editing. **P.-P. De Breuck:** Conceptualization, Formal analysis, Methodology, Software, Visualization, Writing – review & editing. **L. Choisez:** Conceptualization, Investigation, Validation, Writing – review & editing. **M. Marteleur:** Conceptualization, Investigation, Validation, Visualization, Writing – original draft, Writing – review & editing. **M.J. van Setten:** Conceptualization, Formal analysis, Methodology, Software. **G. Petretto:** Formal analysis, Methodology, Software. **G.-M. Rignanese:** Conceptualization, Methodology, Vizualization, Writing – review & editing. **P.J. Jacques:** Conceptualization, Funding acquisition, Methodology, Supervision, Writing – review & editing.

Declaration of competing interest

The authors declare that they have no known competing financial interests or personal relationships that could have appeared to influence the work reported in this paper.

Data availability

Data will be made available on request.

Acknowledgments

The Fonds de la Recherche Scientifique F.R.S.-FNRS (Belgium) is gratefully acknowledged for the grant n°T.0127.19. Computational resources have been provided by the Consortium des Équipements de Calcul Intensif (CÉCI), funded by the Fonds de la Recherche Scientifique de Belgique (F.R.S.-FNRS) under Grant No. 2.5020.11 and by the Walloon Region.

Appendix A. Supplementary data

Supplementary data to this article can be found online at https://doi.org/10.1016/j.matdes.2024.112801.

References

[1] Morinaga, M., Murata, Y., & Yukawa, H., Alloy design based on the DV-Xα cluster method. In *Hartree-Fock-Slater Method for Materials Science*, Springer, Berlin, 2006, pp. 23-48.
[2] M.C. Troparevsky, J.R. Morris, M. Daene, Y. Wang, A.R. Lupini, G.M. Stocks, Beyond atomic sizes and Hume-rothery rules: understanding and predicting high-entropy alloys, JOM 67 (10) (2015) 2350–2363.
[3] U. Mizutani, The Hume-rothery rules for structurally complex alloy phases, Surf. Prop. Eng. Complex Intermet. (2010) 323–399.
[4] M. Morinaga, N. Yukawa, H. Adachi, Alloying effect on the electronic structure of Ni3Al (γ′), J. Phys. Soc. Jpn. 53 (2) (1984) 653–663.
[5] T. Ozaki, H. Matsumoto, S. Watanabe, S. Hanada, β ti alloys with low young's modulus, Mater. Trans. 45 (8) (2004) 2776–2779.
[6] M. Abdel-Hady, K. Hinoshita, M. Morinaga, General approach to phase stability and elastic properties of β-type ti-alloys using electronic parameters, Scr. Mater. 55 (5) (2006) 477–480.
[7] P. Laheurte, F. Prima, A. Eberhardt, T. Gloriant, M. Wary, E. Patoor, Mechanical properties of low modulus β titanium alloys designed from the electronic approach, J. Mech. Behav. Biomed. Mater. 3 (8) (2010) 565–573.
[8] M. Marteleur, F. Sun, T. Gloriant, P. Vermaut, P.J. Jacques, F. Prima, On the design of new β-metastable titanium alloys with improved work hardening rate thanks to simultaneous TRIP and TWIP effects, Scr. Mater. 66 (10) (2012) 749–752.
[9] F. Sun, J.Y. Zhang, M. Marteleur, C. Brozek, E.F. Rauch, M. Veron, P. Vermaut, P. J. Jacques, F. Prima, A new titanium alloy with a combination of high strength, high strain hardening and improved ductility, Scr. Mater. 94 (2015) 17–20.
[10] C. Brozek, F. Sun, P. Vermaut, Y. Millet, A. Lenain, D. Embury, P.J. Jacques, F. Prima, A β-titanium alloy with extra high strain-hardening rate: design and mechanical properties, Scr. Mater. 114 (2016) 60–64.
[11] X.H. Min, K. Tsuzaki, S. Emura, K. Tsuchiya, Enhancement of uniform elongation in high strength Ti–Mo based alloys by combination of deformation modes, Mater. Sci. and Eng.: A 528 (13–14) (2011) 4569–4578.
[12] S. Sadeghpour, S.M. Abbasi, M. Morakabati, A. Kisko, L.P. Karjalainen, D.A. Porter, On the compressive deformation behavior of new beta titanium alloys designed by d-electron method, J. of Alloys and Compd. 746 (2018) 206–217.
[13] A. Zafari, K. Xia, Stress induced martensitic transformation in metastable β ti-5Al-5Mo-5V-3Cr alloy: triggering stress and interaction with deformation bands, Mater. Sci. and Eng.: A 724 (2018) 75–79.
[14] C.H. Wang, A.M. Russell, G.H. Cao, A semi-empirical approach to the prediction of deformation behaviors of β-ti alloys, Scr. Mater. 158 (2019) 62–65.
[15] L.C. Zhang, T. Zhou, S.P. Alpay, M. Aindow, M.H. Wu, Origin of pseudoelastic behavior in Ti–Mo-based alloys, Appl. Phys. Lett. 87 (24) (2005) 241909.
[16] N. Sakaguchi, M. Niinomi, T. Akahori, J. Takeda, H. Toda, Relationships between tensile deformation behavior and microstructure in Ti–Nb–Ta–Zr system alloys, Mater. Sci. and Eng.: C 25 (3) (2005) 363–369.
[17] C. Li, J.H. Chen, X. Wu, W. Wang, S. Van Der Zwaag, Tuning the stress induced martensitic formation in titanium alloys by alloy design, J. of Mater. Sci. 47 (2012) 4093–4100.
[18] M. Bignon, E. Bertrand, F. Tancret, P.E. Rivera-Díaz-del-Castillo, Modelling martensitic transformation in titanium alloys: the influence of temperature and deformation, Materialia 7 (2019) 100382.
[19] S. Neelakantan, D. San Martin, P.E. Rivera-Díaz-del-Castillo, S. van der Zwaag, Plasticity induced transformation in a metastable β ti-1023 alloy by controlled heat treatments, Mater. Sci. Technol. 25 (11) (2009) 1351–1358.
[20] G.H. Zhao, X. Xu, D. Dye, P.E. Rivera-Díaz-del-Castillo, Microstructural evolution and strain-hardening in TWIP ti alloys, Acta Mater. 183 (2020) 155–164.
[21] G. Zhao, X. Li, N. Petrinic, Materials information and mechanical response of TRIP/TWIP ti alloys, Npj Comput. Mater. 7 (1) (2021) 91.
[22] S. Stølen, T. Grande, Chemical thermodynamics of materials: macroscopic and microscopic aspects. s.l, : John Wiley & Sons (2004).
[23] R. Ramprasad, R. Batra, G. Pilania, A. Mannodi-Kanakkithodi, C. Kim, Machine learning in materials informatics: recent applications and prospects, Npj Comput. Mater. 3 (1) (2017) 1–13.
[24] D. Xue, D. Xue, R. Yuan, Y. Zhou, P.V. Balachandran, X. Ding, T. Lookman, An informatics approach to transformation temperatures of NiTi-based shape memory alloys, Acta Mater. 125 (2017) 532–541.
[25] W. Huang, P. Martin, H.L. Zhuang, Machine-learning phase prediction of high-entropy alloys, Acta Mater. 169 (2019) 225–236.
[26] C. Wen, Y. Zhang, C. Wang, D. Xue, Y. Bai, S. Antonov, Y. Su, Machine learning assisted design of high entropy alloys with desired property, Acta Mater. 170 (2019) 109–117.
[27] C. Shen, C. Wang, X. Wei, Y. Li, S. van der Zwaag, W. Xu, Physical metallurgy-guided machine learning and artificial intelligent design of ultrahigh-strength stainless steel, Acta Mater. 179 (2019) 201–214.
[28] N.S. Reddy, J. Krishnaiah, H.B. Young, J.S. Lee, Design of medium carbon steels by computational intelligence techniques, Comput. Mater. Sci. 101 (2015) 120–126.
[29] M.S. Ozerdem, S. Kolukisa, Artificial neural network approach to predict the mechanical properties of Cu–Sn–Pb–Zn–Ni cast alloys, Mater. & Des. 30 (3) (2009) 764–769.
[30] C.T. Wu, H.T. Chang, C.Y. Wu, S.W. Chen, S.Y. Huang, M. Huang, H.W. Yen, Machine learning recommends affordable new ti alloy with bone-like modulus, Materials Today 34 (2020) 41–50.
[31] C.T. Wu, P.H. Lin, S.Y. Huang, Y.J. Tseng, H.T. Chang, S.Y. Li, H.W. Yen, Revisiting alloy design of low-modulus biomedical β-ti alloys using an artificial neural network, Materialia 21 (2022) 101313.
[32] L. Ward, A. Dunn, A. Faghaninia, N.E. Zimmermann, S. Bajaj, Q. Wang, A. Jain, Matminer: an open source toolkit for materials data mining, Comput. Mater. Sci. 152 (2018) 60–69.
[33] P.P. De Breuck, M.L. Evans, G.M. Rignanese, Robust model benchmarking and bias-imbalance in data-driven materials science: a case study on MODNet, J. of Phys.: Condens. Matter 33 (40) (2021) 404002.
[34] J.P. Perdew, K. Burke, M. Ernzerhof, Generalized gradient approximation made simple, Phys. Rev. Lett. 77 (18) (1996) 3865.
[35] G. Kresse, J. Furthmüller, Efficient iterative schemes for ab initio total-energy calculations using a plane-wave basis set, Phys. Rev. B 54 (16) (1996) 11169.
[36] G. Kresse, D. Joubert, From ultrasoft pseudopotentials to the projector augmented-wave method, Phys. Rev. B 59 (3) (1999) 1758.
[37] P.E. Blöchl, Projector augmented-wave method, Phys. Rev. B 50 (24) (1994) 17953.
[38] M. Morinaga, N. Yukawa, T. Maya, K. Sone, H. Adachi, Theoretical design of titanium alloys, In Sixth World Conference on Titanium. III (1998) 1601–1606.
[39] V. Vitek, Intrinsic stacking faults in body-centred cubic crystals, Philosophical Magazine 18 (154) (1968) 773–786.
[40] X. Gonze, J.M. Beuken, R. Caracas, F. Detraux, M. Fuchs, G.M. Rignanese, D. C. Allan, First-principles computation of material properties: the ABINIT software project, Comput. Mater. Sci. 25 (3) (2002) 478–492.
[41] X. Gonze, B. Amadon, P.M. Anglade, J.M. Beuken, F. Bottin, P. Boulanger, J. W. Zwanziger, ABINIT: first-principles approach to material and nanosystem properties, Comput. Phys. Commun. 180 (12) (2009) 2582–2615.
[42] X. Gonze, F. Jollet, F.A. Araujo, D. Adams, B. Amadon, T. Applencourt, J. W. Zwanziger, Recent developments in the ABINIT software package, Comput. Phys. Commun. 205 (2016) 106–131.
[43] D.R. Hamann, X. Wu, K.M. Rabe, D. Vanderbilt, Metric tensor formulation of strain in density-functional perturbation theory, Phys. Rev. B 71 (3) (2005) 035117.
[44] D.R. Hamann, Optimized norm-conserving vanderbilt pseudopotentials, Phys. Rev. B 88 (8) (2013) 085117.
[45] M.J. van Setten, M. Giantomassi, E. Bousquet, M.J. Verstraete, D.R. Hamann, X. Gonze, G.M. Rignanese, The PseudoDojo: training and grading a 85 element optimized norm-conserving pseudopotential table, Comput. Phys. Commun. 226 (2018) 39–54.
[46] Jain, A., Ong, S. P., Chen, W., Medasani, B., Qu, X., Kocher, M., ... & Persson, K. A., FireWorks: A dynamic workflow system designed for high-throughput applications. *Concurr. and Comput.: Pract. and Exp.*, 27(17), (2015) 5037-5059.
[47] Abipy. https://github.com/abinit/abipy.
[48] Abiflows. https://github.com/abinit/abiflows.
[49] S.P. Ong, W.D. Richards, A. Jain, G. Hautier, M. Kocher, S. Cholia, G. Ceder, Python materials genomics (pymatgen): a robust, open-source python library for materials analysis, Comput. Mater. Sci. 68 (2013) 314–319.
[50] K. Mathew, J.H. Montoya, A. Faghaninia, S. Dwarakanath, M. Aykol, H. Tang, A. Jain, Atomate: a high-level interface to generate, execute, and analyze computational materials science workflows, Comput. Mater. Sci. 139 (2017) 140–152.
[51] F.J. Gil, J.M. Guilemany, The determination of the electron to atom ratio interval corresponding to the change in the martensitic structure from α′ to β′ in cuznal shape memory alloys, Materials Research Bulletin 27 (1) (1992) 117–122.
[52] V.A. Chernenko, J. Pons, C. Segu, E. Cesari, Premartensitic phenomena and other phase transformations in Ni–Mn–Ga alloys studied by dynamical mechanical analysis and electron diffraction, Acta Mater. 50 (1) (2002) 53–60.
[53] J.K. Liakos, G.A. Saunders, Application of the Landau theory to elastic phase transitions, Philosophical Magazine A 46 (2) (1982) 217–242.
[54] Gunton, D. J., & Saunders, G. A., Stability limits on the Poisson ratio: application to a martensitic transformation. *Proceedings of the Royal Society of London. A. Mathematical and Physical Sciences*, *343*(1632), (1975) 63-83.
[55] A. Ojha, H. Sehitoglu, Critical stresses for twinning, slip, and transformation in ti-based shape memory alloys, Shape Memory and Superelasticity 2 (2016) 180–195.
[56] S. Hanada, O. Izumi, Deformation behaviour of retained β phase in β-eutectoid ti-cr alloys, J. of Mater. Sci. 21 (12) (1986) 4131–4139.
[57] T. Maeshima, S. Ushimaru, K. Yamauchi, M. Nishida, Effects of sn content and aging conditions on superelasticity in biomedical Ti–Mo–Sn alloys, Mater. Trans. 47 (3) (2006) 513–517.
[58] Y. Takemoto, I. Shimizu, A. Sakakibara, M. Hida, Y. Mantani, Tensile behavior and cold workability of ti-mo alloys, Mater. Trans. 45 (5) (2004) 1571–1576.

[59] M. Abdel-Hady, H. Fuwa, K. Hinoshita, H. Kimura, Y. Shinzato, M. Morinaga, Phase stability change with zr content in β-type Ti–Nb alloys, Scripta Mater 57 (11) (2007) 1000–1003.
[60] K. Otsuka, X. Ren, Recent developments in the research of shape memory alloys, Intermetallics 7 (5) (1999) 511–528.
[61] X. Tang, T. Ahmed, H.J. Rack, Phase transformations in ti-nb-ta and ti-nb-ta-zr alloys, J. Mater. Sci. 35 (2000) 1805–1811.
[62] Y.L. Hao, S.J. Li, S.Y. Sun, R. Yang, Effect of zr and sn on young's modulus and superelasticity of Ti–Nb-based alloys, Mater. Sci. and Eng.: A 441 (1–2) (2006) 112–118.
[63] S. Ishiyama, S. Hanada, O. Izumi, Effect of zr, sn and al additions on deformation mode and beta phase stability of metastable beta ti alloys, ISIJ International 31 (8) (1991) 807–813.
[64] B. Qian, J. Zhang, Y. Fu, F. Sun, Y. Wu, J. Cheng, F. Prima, In-situ microstructural investigations of the TRIP-to-TWIP evolution in ti-mo-zr alloys as a function of zr concentration, J. Mater. Sci. Technol. 65 (2021) 228–237.
[65] http://plasticity.modl-uclouvain.org/.